Available online at www.sciencedirect.com

ScienceDirect

journal homepage: www.elsevier.com/locate/he

Partial crystallization of Co–Fe oxyhydroxides towards enhanced oxygen evolution activity

Xue Bai [a], Yong Fan [b], Changmin Hou [b], Tianmi Tang [a], Jingqi Guan [a,*]

[a] Institute of Physical Chemistry, College of Chemistry, Jilin University, 2519 Jiefang Road, Changchun, 130021, PR China

[b] State Key Laboratory of Inorganic Synthesis and Preparative Chemistry, College of Chemistry, Jilin University, Changchun, 130012, PR China

HIGHLIGHTS

- Partially crystallized $CoFe_{0.8}(OH)_x$ shows higher OER activity than amorphous one.
- $CoFe_{0.8}(OH)_x$ exhibits an overpotential of only 246 mV at 10 mA cm^{-2}.
- Bimetallic $CoFe_{0.8}(OH)_x$ shows lower OER barrier than monometallic counterpart.
- The charge transfer ability can be enhanced by partial crystallization.
- The OER active sites should be di-μ-oxo bridged Fe–Co.

GRAPHICAL ABSTRACT

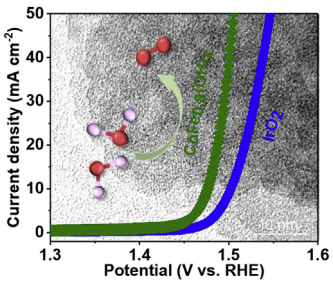

ARTICLE INFO

Article history:
Received 15 January 2022
Received in revised form
18 February 2022
Accepted 19 March 2022
Available online 9 April 2022

Keywords:
Amorphous oxyhydroxide
Cobalt-iron oxyhydroxide
Cobalt-iron oxide
Oxygen evolution reaction
Energy barrier

ABSTRACT

Developing high-performance noble-metal-free electrocatalysts for the oxygen evolution reaction (OER) is of great significance for the large-scale implement of electrochemical water splitting. Here, we demonstrate that cobalt-iron oxyhydroxide ($CoFe_{0.8}(OH)_x$) with appropriate crystallization exhibits excellent OER activity with a low overpotential of only 246 mV, which is much lower than that achieved on amorphous one. Kinetic experiments indicate that the OER active sites should be di-μ-oxo bridged Fe–Co, on which lower energy barrier is attained than that on Fe–O and Co–O sites. Partial crystallization is beneficial to the lattice contraction, the formation of Co–O–Fe sites, and the decrease of charge transfer resistance, thus accelerating OER process.

* *Corresponding author.*
E-mail address: guanjq@jlu.edu.cn (J. Guan).

https://doi.org/10.1016/j.ijhydene.2022.03.174

Introduction

Hydrogen is an ideal energy carrier and one of the most promising alternatives for fossil fuels since the combustion product is water [1–6]. The electrolysis of water is a facile and efficient technique to generate highly pure hydrogen by splitting water into hydrogen and oxygen via two half-reactions: oxygen evolution reaction (OER) hydrogen evolution reaction (HER) [7–11]. Due to slow kinetics and involving 4e transfer, OER is regarded as the rate-determining step of water splitting [12,13]. Although RuO_2 and IrO_2 can catalyze OER well in acidic media, they are unstable in alkaline media [14,15]. Moreover, the scarcity and high cost hinder their large-scale industrial applications [16,17]. Therefore, a lot of investigations have been carried out to develop earth-abundant and cost-efficient transition metal-based catalysts to speed up the sluggish OER [18–25].

The cobalt oxide was theoretically predicted to be very active for the OER, however, the experimental overpotential on CoO_x catalysts is size-dependent [12,26]. In principle, the smaller the CoO_x nanoparticles are, the better the OER activity is. In addition, compared with crystalline cobalt oxide, amorphous CoO_x usually showed higher OER activity due to enhanced stabilization of the O* intermediate on the catalyst surface and increased active sites [26]. Although single-metal Co-based (oxy)hydroxides have been widely investigated for many years, their OER activity is still inferior to commercial iridium oxide, which cannot meet the actual application needs. Therefore, bimetallic Co-based mixed (oxy)hydroxides have received great attention [27]. Various transition metals doped Co-based (oxy)hydroxides were synthesized for the OER, e.g. Cr-doping [28], Fe-doping [29], Ni-doping [30], Mn-doping [31], Cu-doping [32], Sb-doping [33], Mo-doping [34], Ce-doping [35], Ru-doping [36], and Ir-doping [37]. Thereinto, Fe-doping is a very efficient strategy to significantly improve the OER performance of Co-based electrocatalysts due to a cooperation mechanism between Fe and Co during the reaction [29,38].

For Co–Fe (oxy)hydroxides, the OER performance is greatly influenced by the structure [39–41]. For example, Sargent et al. found that a gelled FeCo oxyhydroxide exhibited an OER overpotential (η_{10}) of 277 mV at 10 mA cm^{-2} [42]. Zhu et al. reported that ultrathin $CoFeO_x$ nanosheets with thickness of 1.2 nm and abundant oxygen vacancies showed an η_{10} of 350 mV [43]. Zeng et al. found that crystalline CoFe nanoparticles wrapped in N-doped carbon nanotubes exhibited an η_{10} of 292 mV [44]. We found that a core-shell Co_3O_4@FeO_x catalyst displayed higher OER activity than CoFe-mixed oxides, which was ascribed to better ability to bind water molecules on Fe sites and improved charge transfer ability [45]. Furthermore, we found that a mesoporous $CoFe_{0.05}O_x$ demonstrated an η_{10} of 280 mV due to a cooperation mechanism between Fe and Co sites to lower the OER barrier [46]. Compared with crystalline metal oxides, amorphous counterparts showed higher OER activity [47]. However, amorphous mixed metal oxides usually exhibit larger resistance than crystalline ones due to irregular atomic distribution, resulting in poor charge transfer property [48]. Therefore, it is

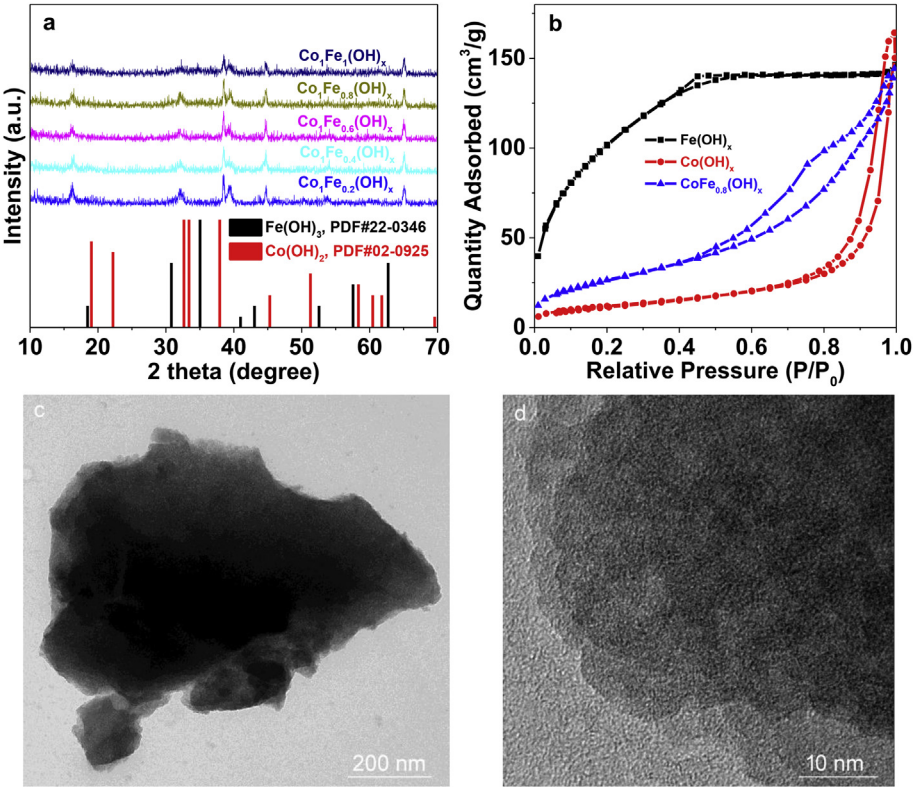

Fig. 1 – XRD patterns of $CoFe_n(OH)_x$ and referred samples. (b) N_2 adsorption–desorption isotherms of $Fe(OH)_x$, $Co(OH)_x$, and $CoFe_{0.8}(OH)_x$. (c) TEM image of $CoFe_{0.8}(OH)_x$. (d) HRTEM image of $CoFe_{0.8}(OH)_x$.

advisable to design partially crystallized materials combining the merits of good charge transfer ability in crystalline mixed metal oxides and high OER activity of amorphous mixed metal oxides [49].

Here, we fabricated partially crystallized Co–Fe oxyhydroxides for enhanced OER activity. Compared with amorphous Co–Fe oxyhydroxides, partially crystallized ones show higher OER activity due to faster charge transfer and lower reaction barrier. According to the kinetic studies, single-component Fe/Co oxyhydroxide exhibits much higher OER barrier than Co–Fe oxyhydroxides, indicating that the efficient active site should be Fe–O–Co species.

Results and discussion

Partially crystallized Co–Fe oxyhydroxides were synthesized by drying the gelled Co–Fe at 40 °C, which were nominated as $CoFe_n(OH)_x$ (n = 0.2, 0.4, 0.6, 0.8, and 1), while amorphous $CoFe_{0.8}(OH)_x$ oxyhydroxide was synthesized by a vacuum freeze-drying method, which was donated as CoFe-AO. As displayed in Fig. 1a, there are obvious peaks at around 16.1, 32.1, 38.4, 39.4, 44.8, and 65.1° for the $CoFe_n(OH)_x$, which should be ascribed to a bimetallic CoFe-oxyhydroxide. However, it should be noted that these peaks are very weak, indicating low degree of crystallinity. As a contrast, no obvious diffraction peaks can be observed for the CoFe-AO (Fig. S1), indicating its amorphous state. The BET specific area for the $Fe(OH)_x$, $Co(OH)_x$, and $CoFe_{0.8}(OH)_x$ is 390.1, 43.9, and 99.2 $m^2\ g^{-1}$, respectively (Fig. 1b). From Fig. 1c, irregular blocky structure is typically observed for the $CoFe_{0.8}(OH)_x$. From HRTEM image (Fig. 1d), partially crystallized structure can be observed at the edges, which is in good agreement with the XRD results. The partially crystallized structure in the $CoFe_{0.8}(OH)_x$ can be further verified by SAED pattern (Fig. S2). From SEM-EDS mappings (Fig. 2), the Fe and Co elements are well dispersed in the $CoFe_{0.8}(OH)_x$. Moreover, porous structure can be observed for $Fe(OH)_x$, $Co(OH)_x$, and $CoFe_{0.8}(OH)_x$ (Fig. 2 and Fig. S3).

The elemental composition and the oxidation state of the $CoFe_{0.8}(OH)_x$ were analyzed by XPS. XPS survey spectrum of $CoFe_{0.8}(OH)_x$ confirms the existence of Fe, Co, O, C, and Cl elements (Fig. 3a). Combined with the aforementioned SEM-EDX results, it can be inferred that the C element comes from

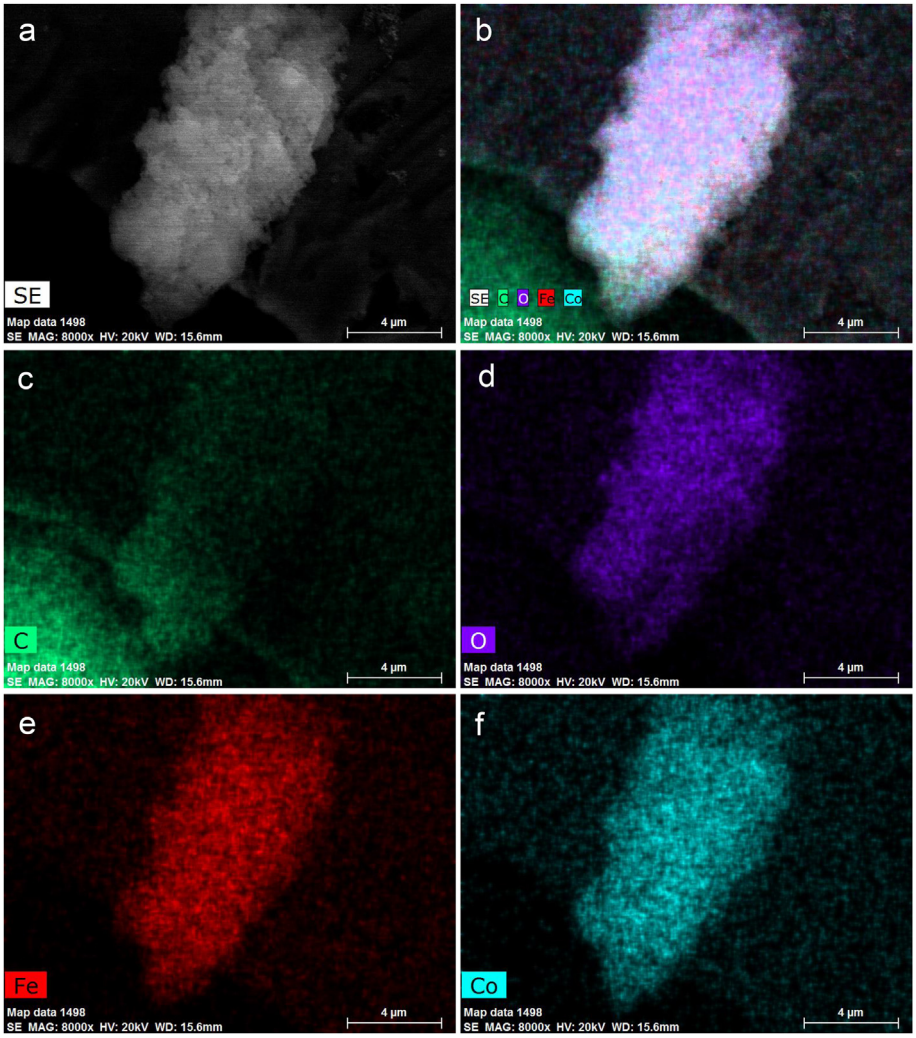

Fig. 2 – (a) SEM image of $CoFe_{0.8}(OH)_x$. (b–f) EDX mappings.

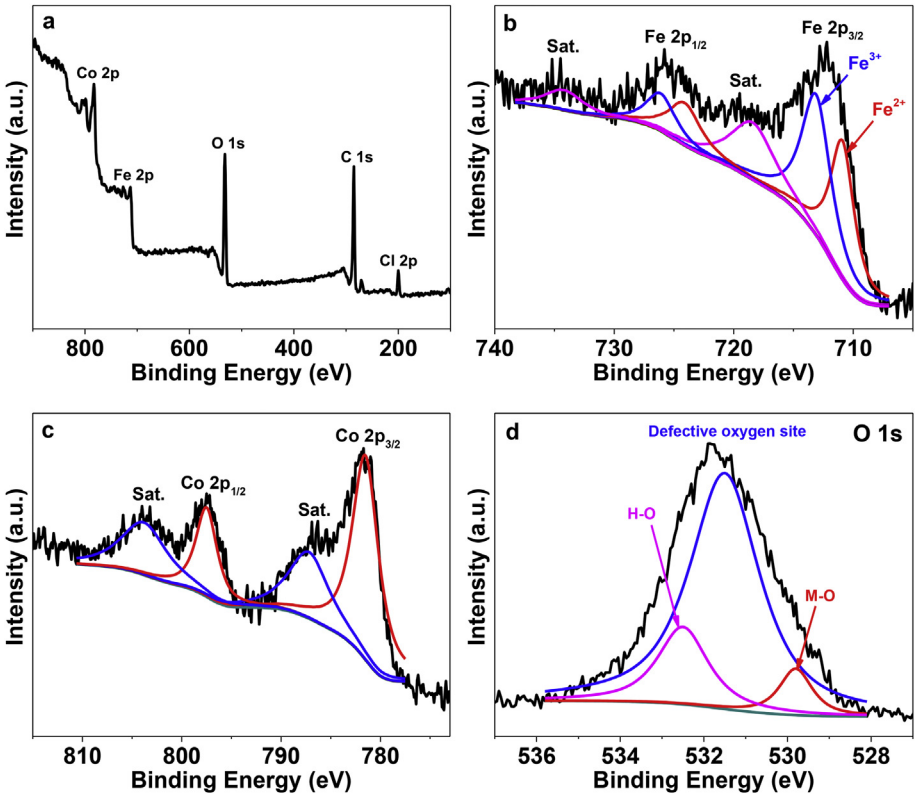

Fig. 3 – (a) XPS survey spectrum of $CoFe_{0.8}(OH)_x$. (b–d) High-resolution Fe 2p, Co 2p, and O 1s XPS spectra, respectively.

polluting carbon sources in the XPS analysis, while the Cl element was absorbed on the catalyst during the synthetic procedure. For the Fe element (Fig. 3b), the Fe $2p_{3/2}$ peak can be split into Fe^{2+} $2p_{3/2}$ (710.9 eV) and Fe^{3+} $2p_{3/2}$ (713.1 eV) peaks [50]. The relative surface content of Fe^{3+}/Fe^{2+} is estimated to be ca. 1.3:1. For the Co element (Fig. 3c), two peaks are located at 781.6 (Co^{2+} $2p_{3/2}$) and 797.6 eV (Co^{2+} $2p_{1/2}$) along with two satellite peaks [51]. For the O element (Fig. 3d), the O 1s peak can be

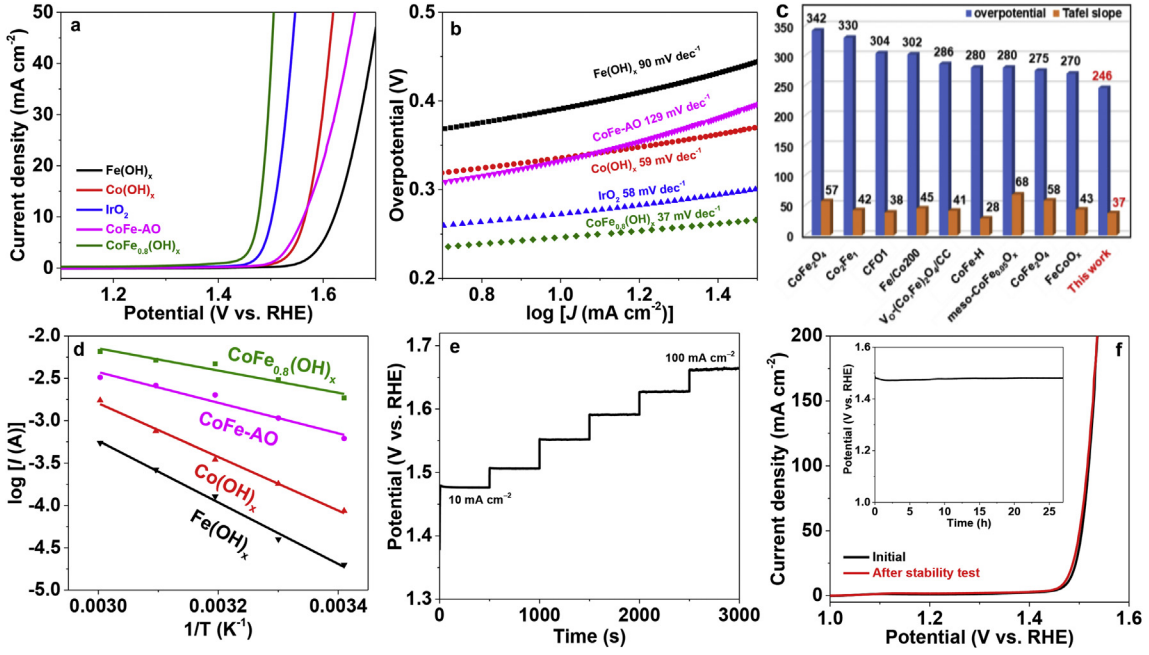

Fig. 4 – (a) Polarization curves. (b) Tafel slopes. (c) Comparisons of overpotentials at 10 mA cm^{-2} and Tafel slopes. (d) Arrhenius plots of the kinetic current at $\eta = 300$ mV without iR compensation. (e) Multi-current electrochemical process of $CoFe_{0.8}(OH)_x$. (f) Polarization curves of $CoFe_{0.8}(OH)_x$ before and after stability test. Inset: Chronopotentiometry curve of $CoFe_{0.8}(OH)_x$ at a current density of 10 A cm^{-2}.

fitted into three well-defined peaks centered at 532.5 (–OH), 531.5 (defective O site), and 529.8 eV (Fe/Co–O) [28,45,52,53].

The electrocatalytic OER activity of $CoFe_{0.8}(OH)_x$ was investigated in 1.0 M KOH using a standard three-electrode system with glassy carbon electrode as the working electrode. For comparison, $Fe(OH)_x$, $Co(OH)_x$, amorphous $CoFe_{0.8}$ oxyhydroxide (CoFe-AO), and IrO_2 were also tested under similar conditions. Among them, $CoFe_{0.8}(OH)_x$ exhibited the best OER performance with the smallest overpotential (η_{10}) of 246 mV at 10 mA cm^{-1} and the largest electrocatalytic current through the whole potential range (Fig. 4a), which is lower than the η_{10} of $Fe(OH)_x$ (391 mV), $Co(OH)_x$ (335 mV), CoFe-AO (332 mV), and IrO_2 (272 mV), indicating the essential effect of concerted catalysis between Fe and Co and their microenvironment. We further investigated the influence of the molar ratio of Fe/Co on the OER performance. The OER activity increases gradually with increasing the Fe/Co molar ratio and reaches a maximum at Fe/Co = 0.8:1 (Fig. S4). Further increasing the Fe/Co molar ratio would result in the decrease of OER performance. The Tafel slope of $CoFe_{0.8}(OH)_x$ is measured as 37 mV dec^{-1} (Fig. 4b), which is smaller than that of $Fe(OH)_x$ (90 mV), $Co(OH)_x$ (59 mV), CoFe-AO (129 mV), and IrO_2 (58 mV), indicating more favorable kinetics for the OER. The η_{10} on the $CoFe_{0.8}(OH)_x$ is lower than most CoFe-based electrocatalysts for OER reported (Fig. 4c and Table S1), for instance, defect-rich V_O-(Co, Fe)$_3O_4$/CC (η_{10} = 286 mV) [54], *meso*-$CoFe_{0.05}O_x$ (η_{10} = 280 mV) [46], porous CFO1 nanoplates (η_{10} = 304 mV) [55], Co_2Fe_1 (η_{10} = 330 mV) [56], Fe/Co200 (η_{10} = 302 mV) [57], mesoporous $CoFe_2O_4$ (η_{10} = 342 mV) [58], $CoFe_2O_4$ nanospheres (η_{10} = 275 mV) [59], and amorphous CoFe–H (η_{10} = 280 mV) [60].

To evaluate the OER barrier on these catalysts, we investigated the influence of temperature on the electrocatalytic activity (Fig. S5). The OER activity increases with elevating the temperature, suggesting that the chemical rate constant is relative to the temperature. The kinetic barrier can be calculated using the Arrhenius plots at η = 300 mV (Fig. S5) [42,61]. The $CoFe_{0.8}(OH)_x$ displays a low kinetic barrier of 25.1 kJ mol^{-1} (Fig. 4d), much smaller than $Fe(OH)_x$ (69.5 kJ mol^{-1}), $Co(OH)_x$ (60.5 kJ mol^{-1}), and CoFe-AO (34.6 kJ mol^{-1}), reflecting more favorable OER kinetics on the $CoFe_{0.8}(OH)_x$. Since monometallic Fe/Co oxyhydroxides show much higher kinetic barrier than bimetallic CoFe oxyhydroxides, the efficient active site for the OER should be di-μ-oxo bridged Fe–Co sites [29].

The electrocatalytic active sites of the catalysts were estimated from the electrochemical double-layer capacitance (Fig. S6). The $CoFe_{0.8}(OH)_x$ exhibits a double-layer capacitance (C_{dl}) value of 4.68 mF cm^{-2}, 10.4-fold higher than CoFe-AO under the same conditions, reflecting much more available active sites in the former. Partial crystallization of CoFe oxyhydroxides favors the lattice contraction and the formation of di-μ-oxo bridged Fe–Co sites, thus increasing active sites. Moreover, the C_{dl} increases with increasing the Fe/Co molar ratio and reaches a maximum at Fe/Co = 0.8. Further increasing the Fe/Co molar ratio would lead to the decrease of C_{dl} value, suggesting that the $CoFe_{0.8}(OH)_x$ possesses the most active sites in the $CoFe_n(OH)_x$ samples. The charge transfer ability of the catalysts was studied by electrochemical impedance spectrum (EIS) test (Fig. S7). The charge transfer resistance for $CoFe_{0.8}(OH)_x$, CoFe-AO, $Co(OH)_x$, and $Fe(OH)_x$ is 56, 0.8, 17.6, and 0.5 Ω cm^2, respectively. Compared

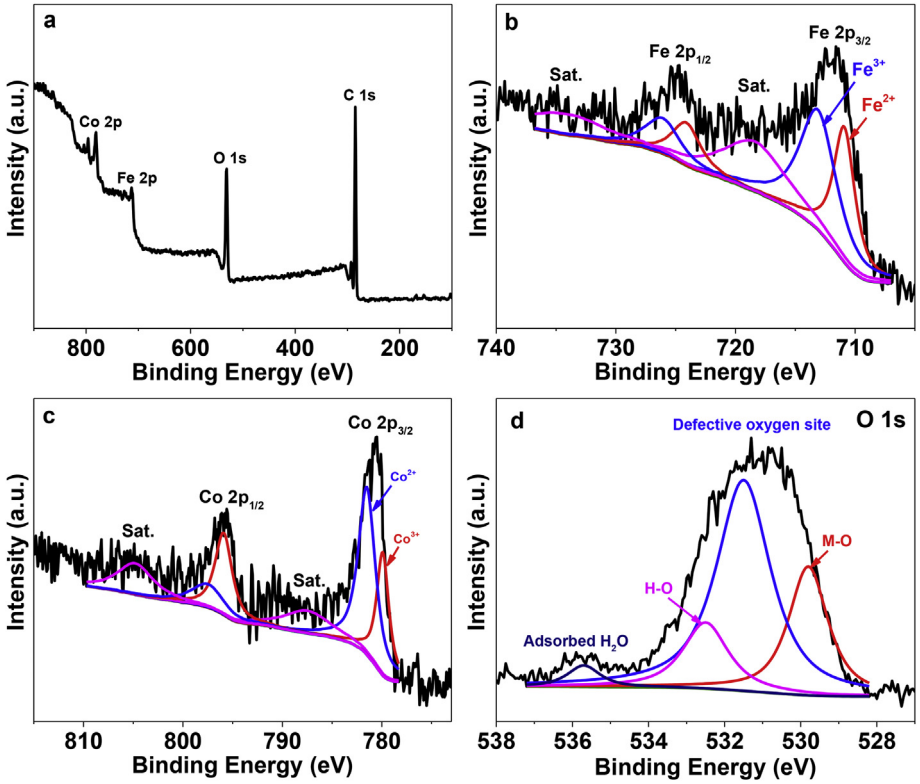

Fig. 5 – XPS survey spectrum (a), and high-resolution XPS spectra of Fe 2p (b), Co 2p (c), and O 1s (d) of the used $CoFe_{0.8}(OH)_x$.

with amorphous CoFe-AO, partially crystallized $CoFe_{0.8}(OH)_x$ exhibits much smaller resistance of charge transfer, manifesting more favorable OER kinetics.

The durability of $CoFe_{0.8}(OH)_x$ was first evaluated multistep chronopotentiometric measurement (Fig. 4e). The potentials immediately level out at a series of current density ranged from 10 to 100 mA cm^{-2} and remain constant for the residual 500 s, demonstrating that the excellent mass transport ability and robust water oxidation performance of the $CoFe_{0.8}(OH)_x$. The durability of $CoFe_{0.8}(OH)_x$ was further assessed by long-time chronopotentiometric measurement at 10 mA cm^{-2} (inset in Fig. 4f), revealing that the $CoFe_{0.8}(OH)_x$ retains its catalytic activity over 27 h. The polarization curve of the $CoFe_{0.8}(OH)_x$ after the chronopotentiometric test exhibits no obvious loss (Fig. 4f), implying excellent electrocatalytic OER stability.

The surface compositions and metal valence state of the $CoFe_{0.8}(OH)_x$ after OER stability measurement were investigated by XPS (Fig. 5). The XPS survey spectrum reveals the existence of Fe, Co, O, and C in the used $CoFe_{0.8}(OH)_x$ (Fig. 5a). The relative surface content of Fe^{3+}/Fe^{2+} increases from 1.3:1 in the fresh sample to 1.5:1 in the used sample (Fig. 5b), indicating that the Fe should be involved in the OER process. Moreover, Co^{3+} ions were generated after OER test and the relative surface content of Co^{3+}/Co^{2+} is calculated to be 0.53:1 (Fig. 5c), demonstrating that Co ions also took part in the OER process. Furthermore, the surface oxygen species kept dynamic condition during the OER (Fig. 5d).

Conclusions

In summary, we demonstrate that partially crystallized $CoFe_{0.8}(OH)_x$ oxyhydroxide exhibited excellent OER activity with an η_{10} of only 246 mV, which is much lower than amorphous CoFe-AO. Kinetic studies revealed that di-μ-oxo bridged Fe–Co sites should be the active sites for efficient OER, over which lower kinetic energy barrier can be achieved than that on single metallic Fe/Co oxyhydroxide. Appropriate crystallization favored the lattice contraction, the generation of Fe–O–Co sites, and the improvement of charge transfer ability, thus promoting OER activity. This work may provide new insights into the design of This work may provide new insights into the design of high-performance transition-metal-based OER catalysts towards energy-related applications.

Declaration of competing interest

The authors declare that they have no known competing financial interests or personal relationships that could have appeared to influence the work reported in this paper.

Acknowledgments

This work was supported by the National Natural Science Foundation of China (22075099) and the Education Department of Jilin Province (JJKH20220967KJ).

Appendix A. Supplementary data

Supplementary data to this article can be found online at https://doi.org/10.1016/j.ijhydene.2022.03.174.

REFERENCES

[1] Li S, Sun J, Guan J. Strategies to improve electrocatalytic and photocatalytic performance of two-dimensional materials for hydrogen evolution reaction. Chin J Catal 2021;42:511–56.
[2] Wang X, Zheng Y, Sheng W, Xu ZJ, Jaroniec M, Qiao S-Z. Strategies for design of electrocatalysts for hydrogen evolution under alkaline conditions. Mater Today 2020;36:125–38.
[3] Su P, Pei W, Wang X, Ma Y, Jiang Q, Liang J, et al. Exceptional electrochemical HER performance with enhanced electron transfer between Ru nanoparticles and single atoms dispersed on a carbon substrate. Angew Chem Int Ed 2021;60:16044–50.
[4] Boyjoo Y, Wang M, Pareek VK, Liu J, Jaroniec M. Synthesis and applications of porous non-silica metal oxide submicrospheres. Chem Soc Rev 2016;45:6013–47.
[5] Gong F, Ye S, Liu M, Zhang J, Gong L, Zeng G, et al. Boosting electrochemical oxygen evolution over yolk-shell structured O–MoS2 nanoreactors with sulfur vacancy and decorated Pt nanoparticles. Nano Energy 2020;78:105284.
[6] Gong F, Liu M, Ye S, Gong L, Zeng G, Xu L, et al. All-pH stable sandwich-structured MoO2/MoS2/C hollow nanoreactors for enhanced electrochemical hydrogen evolution. Adv Funct Mater 2021;31:2101715.
[7] Song J, Wei C, Huang Z-F, Liu C, Zeng L, Wang X, et al. A review on fundamentals for designing oxygen evolution electrocatalysts. Chem Soc Rev 2020;49:2196–214.
[8] Zhao D, Zhuang Z, Cao X, Zhang C, Peng Q, Chen C, et al. Atomic site electrocatalysts for water splitting, oxygen reduction and selective oxidation. Chem Soc Rev 2020;49:2215–64.
[9] Yan D, Zhang L, Chen Z, Xiao W, Yang X. Nickel-based metal-organic framework-derived bifunctional electrocatalysts for hydrogen and oxygen evolution reactions. Acta Phys Chim Sin 2021;37:2009054.
[10] Li P, Hong W, Liu W. Fabrication of large scale self-supported WC/Ni(OH)(2) electrode for high-current-density hydrogen evolution. Chin J Struct Chem 2021;40:1365–71.
[11] Wu Y, Xie N, Li X, Fu Z, Wu X, Zhu Q. MOF-derived hierarchical hollow NiRu-C nanohybrid for efficient hydrogen evolution reaction. Chin J Struct Chem 2021;40:1346–56.
[12] Man IC, Su H-Y, Calle-Vallejo F, Hansen HA, Martinez JI, Inoglu NG, et al. Universality in oxygen evolution electrocatalysis on oxide surfaces. ChemCatChem 2011;3:1159–65.
[13] Sun H, Yan Z, Liu F, Xu W, Cheng F, Chen J. Self-supported transition-metal-based electrocatalysts for hydrogen and oxygen evolution. Adv Mater 2020;32:1806326.
[14] Li Y, Sun Y, Qin Y, Zhang W, Wang L, Luo M, et al. Recent advances on water-splitting electrocatalysis mediated by noble-metal-based nanostructured materials. Adv Energy Mater 2020;10:1903120.
[15] Lei Z, Wang T, Zhao B, Cai W, Liu Y, Jiao S, et al. Recent progress in electrocatalysts for acidic water oxidation. Adv Energy Mater 2020;10:2000478.
[16] Huang Z-F, Song J, Dou S, Li X, Wang J, Wang X. Strategies to break the scaling relation toward enhanced oxygen electrocatalysis. Matter 2019;1:1494–518.

[17] Liu Y, Li W, Wu H, Lu S. Carbon dots enhance ruthenium nanoparticles for efficient hydrogen production in alkaline. Acta Phys Chim Sin 2021;37:2009082.
[18] Lyu F, Wang Q, Choi SM, Yin Y. Noble-metal-free electrocatalysts for oxygen evolution. Small 2019;15:1804201.
[19] Wang J, Xu F, Jin H, Chen Y, Wang Y. Non-noble metal-based carbon composites in hydrogen evolution reaction: fundamentals to applications. Adv Mater 2017;29:1605838.
[20] Xu B, Zhang Y, Pi Y, Shao Q, Huang X. Research progress of nickel-based metal-organic frameworks and their derivatives for oxygen evolution catalysis. Acta Phys Chim Sin 2021;37:2009074.
[21] Gao Z, Wang C, Li J, Zhu Y, Zhang Z, Hu W. Conductive metal-organic frameworks for electrocatalysis: achievements, challenges, and opportunities. Acta Phys Chim Sin 2021;37:2010025.
[22] Guan J, Bai X, Tang T. Recent progress and prospect of carbon-free single-site catalysts for the hydrogen and oxygen evolution reactions. Nano Res 2022;15:818–37.
[23] Fu C-L, Wang Y, Huang J-H. Hybrid of quaternary layered double hydroxides and carbon nanotubes for oxygen evolution reaction. Chin J Struct Chem 2020;39:1807–16.
[24] Jia Q-Q, Li J-Y, Zhang H-X, Chen L-Z, Wang G-X. Synthesis, crystal structure and properties of a copper(I) coordination polymer based on benzimidazole derivative. Chin J Struct Chem 2020;39:2021–6.
[25] Yu Y-M, Liu J-J, Qi R, Zuo C-J, Zhao W-G, Lu J-L, et al. Interface-reconstruction forming bifunctional (LixTM1-x)O rock-salt shell for enhanced cyclability in Li-rich layered oxide. Chin J Struct Chem 2020;39:1363–71.
[26] Chen Z, Duan Z, Wang Z, Liu X, Gu L, Zhang F, et al. Amorphous cobalt oxide nanoparticles as active water-oxidation catalysts. ChemCatChem 2017;9:3641–5.
[27] Zhao K, Li X, Su D. High-entropy alloy nanocatalysts for electrocatalysis. Acta Phys Chim Sin 2021;37:2009077.
[28] Dong C, Yuan X, Wang X, Liu X, Dong W, Wang R, et al. Rational design of cobalt-chromium layered double hydroxide as a highly efficient electrocatalyst for water oxidation. J Mater Chem A 2016;4:11292–8.
[29] Smith RDL, Pasquini C, Loos S, Chernev P, Klingan K, Kubella P, et al. Spectroscopic identification of active sites for the oxygen evolution reaction on iron-cobalt oxides. Nat Commun 2017;8:2022.
[30] Bae S-H, Kim J-E, Randriamahazaka H, Moon S-Y, Park J-Y, Oh I-K. Seamlessly conductive 3D nanoarchitecture of core-shell Ni-Co nanowire network for highly efficient oxygen evolution. Adv Energy Mater 2017;7:1601492.
[31] Song F, Hu X. Ultrathin cobalt-manganese layered double hydroxide is an efficient oxygen evolution catalyst. J Am Chem Soc 2014;136:16481–4.
[32] Lopez-Fernandez E, Gil-Rostra J, Espinos JP, Gonzalez-Elipe AR, Yubero F, de Lucas-Consuegra A. CuxCo3-xO4 ultra-thin film as efficient anodic catalysts for anion exchange membrane water electrolysers. J Power Sources 2019;415:136–44.
[33] Ham K, Hong S, Kang S, Cho K, Lee J. Extensive active-site formation in trirutile CoSb2O6 by oxygen vacancy for oxygen evolution reaction in anion exchange membrane water splitting. ACS Energy Lett 2021;6:364–70.
[34] Kuznetsov DA, Konev DV, Sokolov SA, Fedyanin IV. Cobalt oxide materials for oxygen evolution catalysis via single-source precursor chemistry. Chem Eur J 2018;24:13890–6.
[35] Pan L, Wang Q, Li Y, Zhang C. Amorphous cobalt-cerium binary metal oxides as high performance electrocatalyst for oxygen evolution reaction. J Catal 2020;384:14–21.
[36] Liu Y, Zhao W, Zhang X. Soft template synthesis of mesoporous Co3O4/RuO2 center dot xH(2)O composites for electrochemical capacitors. Electrochim Acta 2008;53:3296–304.
[37] Cai C, Wang M, Han S, Wang Q, Zhang Q, Zhu Y, et al. Ultrahigh oxygen evolution reaction activity achieved using Ir single atoms on amorphous CoOx nanosheets. ACS Catal 2021;11:123–30.
[38] Enman LJ, Stevens MB, Dahan MH, Nellist MR, Toroker MC, Boettcher SW. Operando X-ray absorption spectroscopy shows iron oxidation is concurrent with oxygen evolution in cobalt-iron (oxy)hydroxide electrocatalysts. Angew Chem Int Ed 2018;57:12840–4.
[39] Babar P, Lokhande A, Shin HH, Pawar B, Gang MG, Pawar S, et al. Cobalt iron hydroxide as a precious metal-free bifunctional electrocatalyst for efficient overall water splitting. Small 2018;14:1702568.
[40] Patil K, Babar P, Bae H, Jo E, Jang JS, Bhoite P, et al. Enhanced electrocatalytic activity of a layered triple hydroxide (LTH) by modulating the electronic structure and active sites for efficient and stable urea electrolysis. Sustain Energy Fuels 2022;6:474–83.
[41] Babar P, Patil K, Mahmood J, Kim S, Kim JH, Yavuz CT. Low overpotential overall water splitting by a cooperative interface of cobalt-iron hydroxide and iron oxyhydroxide. Cell Rep Phys Sci 2022;3:100762.
[42] Zhang B, Zheng X, Voznyy O, Comin R, Bajdich M, García-Melchor M, et al. Homogeneously dispersed multimetal oxygen-evolving catalysts. Science 2016;352:333–7.
[43] Zhuang L, Ge L, Yang Y, Li M, Jia Y, Yao X, et al. Ultrathin iron-cobalt oxide nanosheets with abundant oxygen vacancies for the oxygen evolution reaction. Adv Mater 2017;29:1606793.
[44] Zeng X, Jang MJ, Choi SM, Cho H-S, Kim C-H, Myung NV, et al. Single-crystalline CoFe nanoparticles encapsulated in N-doped carbon nanotubes as a bifunctional catalyst for water splitting. Mater Chem Front 2020;4:2307–13.
[45] Liu N, Guan J. Core-shell Co3O4@FeOx catalysts for efficient oxygen evolution reaction. Mater Today Energy 2021;21:100715.
[46] Tang T, Zhang Q, Bai X, Wang Z, Guan J. Enhanced oxygen evolution activity on mesoporous cobalt-iron oxides. Chem Commun 2021;57:11843–6.
[47] Smith RD, Prévot MS, Fagan RD, Zhang Z, Sedach PA, Siu MKJ, et al. Photochemical route for accessing amorphous metal oxide materials for water oxidation catalysis. Science 2013;340:60–3.
[48] Tong Y, Guo H, Liu D, Yan X, Su P, Liang J, et al. Vacancy engineering of iron-doped W18O49 nanoreactors for low-barrier electrochemical nitrogen reduction. Angew Chem Int Ed 2020;59:7356–61.
[49] Zhang Q, Guan J. Applications of single-atom catalysts. Nano Res 2022;15:38–70.
[50] Wei H-l, Tan A-d, Hu S-z, Piao J-h, Fu Z-y. Efficient spinel iron-cobalt oxide/nitrogen-doped ordered mesoporous carbon catalyst for rechargeable zinc-air batteries. Chin J Catal 2021;42:1451–8.
[51] Zhang X, Jin M, Lian Q, Peng O, Niu S, Ai Z, et al. Ion modification of transition cobalt oxide by soaking strategy for enhanced water splitting. Chem Eng J 2021;423:130218.
[52] Zhang Q, Liu N, Guan J. Charge-transfer effects in Fe-Co and Fe-Co-Y oxides for electrocatalytic water oxidation reaction. ACS Appl Energy Mater 2019;2:8903–11.
[53] Li Y, Lu M, Wu Y, Ji Q, Xu H, Gao J, et al. Morphology regulation of metal-organic framework-derived

nanostructures for efficient oxygen evolution electrocatalysis. J Mater Chem A 2020;8:18215–9.
[54] Liu F, Jin W, Li Y, Zheng L, Hu Y, Xu X, et al. Defect-rich (Co, Fe)(3)O-4 hierarchical nanosheet arrays for efficient oxygen evolution reaction. Appl Surf Sci 2020;529:147125.
[55] Lyu F, Bai Y, Wang Q, Wang L, Zhang X, Yin Y. Coordination-assisted synthesis of iron-incorporated cobalt oxide nanoplates for enhanced oxygen evolution. Mater Today Chem 2019;11:112–8.
[56] Chen G-C, Wondimu TH, Huang H-C, Wang K-C, Wang C-H. Microwave-assisted facile synthesis of cobalt-iron oxide nanocomposites for oxygen production using alkaline anion exchange membrane water electrolysis. Int J Hydrogen Energy 2019;44:10174–81.
[57] Huang Y, Yang R, Anandhababu G, Xie J, Lv J, Zhao X, et al. Cobalt/iron(oxides) heterostructures for efficient oxygen evolution and benzyl alcohol oxidation reactions. ACS Energy Lett 2018;3:1854–60.
[58] Huang Y, Yang W, Yu Y, Hao S. Ordered mesoporous spinel CoFe2O4 as efficient electrocatalyst for the oxygen evolution reaction. J Electroanal Chem 2019;840:409–14.
[59] Guo D, Kang H, Wei P, Yang Y, Hao Z, Zhang Q, et al. A high-performance bimetallic cobalt iron oxide catalyst for the oxygen evolution reaction. CrystEngComm 2020;22:4317–23.
[60] Liu W, Liu H, Dang L, Zhang H, Wu X, Yang B, et al. Amorphous cobalt-iron hydroxide nanosheet electrocatalyst for efficient electrochemical and photo-electrochemical oxygen evolution. Adv Funct Mater 2017;27:1603904.
[61] Swierk JR, Klaus S, Trotochaud L, Bell AT, Tilley TD. Electrochemical study of the energetics of the oxygen evolution reaction at nickel iron (oxy)hydroxide catalysts. J Phys Chem C 2015;119:19022–9.